J Mater Sci: Mater Med (2010) 21:1151–1161
DOI 10.1007/s10856-009-3983-y

Fretting wear behavior of calcium phosphate-mullite composites in dry and albumin-containing simulated body fluid conditions

Shekhar Nath · Raghunandan Ummethala · Bikramjit Basu

Received: 7 October 2009 / Accepted: 23 December 2009 / Published online: 7 January 2010

Abstract In a recent work, it has been shown that it is possible to achieve a better combination of compressive strength, flexural strength and toughness properties in calcium phosphate (CaP) composites containing 20 and 30 wt% mullite ($3Al_2O_3{\cdot}2SiO_2$). In view of their potential application as load bearing implants, the present work reports the friction and wear properties of the newly developed composites against zirconia under dry ambient as well as in simulated body fluid (SBF) containing bovine serum albumin (BSA) protein. For comparison, experiments were also conducted on monolithic hydroxyapatite (HAp, $Ca_{10}(PO_4)_6(OH)_2$) and mullite under identical conditions. Under the investigated fretting conditions, the mullite-containing composites exhibited higher coefficient of friction (COF) of 0.4–0.6, compared to pure HAp (COF $\sim$ 0.25–0.3). Although the wear resistance of the composites containing 20 or 30 wt% mullite was better in dry conditions, higher wear rate was measured in SBF conditions. The difference in tribological properties has been analyzed in reference to the difference in phase assemblage and mechanical properties. A comparison with some competing biomaterials reveals good potential of the investigated CaP-mullite composites for application as wear resistant implants.

S. Nath · R. Ummethala · B. Basu (✉)
Laboratory for Biomaterials, Materials and Metallurgical Engineering, Indian Institute of Technology Kanpur, Kanpur 208016, UP, India
e-mail: bikram@iitk.ac.in

1 Introduction

Calcium phosphate based materials are now being widely investigated due to their excellent biocompatibility properties [1–4]. However, the use of monolithic CaP materials has been limited due to their poor fracture resistance. Therefore, the composites based on CaP materials are of great interest. Till date, various HAp and other CaP based composites have been being developed and widely reported [5–10]. In a recent investigation [11–13], a novel CaP-mullite composite has been developed for biomedical applications. These CaP-mullite composites have showed a good combination of SEVNB fracture toughness (1.5 MPa $m^{0.5}$), compressive strength ($\sim$300 MPa) and biocompatibility.

Mullite is a solid solution of alumina and silica and is the most stable phase among the aluminosilicate group of materials. In the earlier in vitro and in vivo studies [12, 13], it has been proved that mullite-containing (up to 30 wt%) calcium phosphate composite is as biocompatible as pure HAp. Also, calcium-phosphate—mullite composites possess better fracture toughness (2.5 times higher than HAp) at the same time maintain lower Young's modulus values ($\sim$70 GPa) [12]. Among various properties, the wear behavior of the developed composites should be evaluated in the light of its potential use in different contacting surfaces. One of the ways of testing the wear properties of the materials would be the fretting test, since it is one of the mechanisms by which the implant undergoes wear at the joints. In order to have a closer simulation of the physiological conditions, the fretting tests were carried out in a simulated body fluid with or without proteins.

Schaaff [14] discussed in his review article about the role of fretting damage in total hip arthroplasty. It was reported that the fretting damage had been mainly observed at the contact surface between two parts joined together (taper

junction, neck). The fretting damage led to material removal as well as release of ions, which might cause allergies, toxic reaction, osteolysis, septic and aseptic loosening, resulting in negative clinical outcomes leading to revision surgery. However, it was mentioned that good design of the prosthetic implant might reduce the fretting damage to a great extent. Therefore, in addition to tailoring the design aspect, it is important to develop materials with good resistance to fretting wear. Fu et al. [15] studied the fretting wear behavior of thermal sprayed hydroxyapatite coating lubricated with bovine albumin. They reported COF value of 0.7–0.8 for unlubricated condition, whereas much lower COF of 0.2–0.3 was recorded in lubricating condition. They concluded that bovine albumin had created effective lubrication during fretting. The main wear mechanisms were delamination, pitting and abrasive wear. In view of concerns over wear-induced failure of biomaterials, a number of studies evaluated the friction and wear of diverse implant materials both in dry conditions as well as in the simulated body fluid environment [16–25].

In view of favorable combination of physical and biological properties, various mullite-containing (10–30 wt%) CaP-composites were investigated in the present work under fretting contact against zirconia counterbody in ball-on-flat configuration. Zirconia being harder and tougher than the developed composites was expected to cause damage to the composites. The fretting experiments were carried out in dry ambient condition as well as in albumin-containing simulated body fluid (SBF) medium. To compare the results, the tribological properties of pure HAp and pure mullite samples were selected as baseline samples.

2 Experimental

For the purpose of producing composites, HAp was synthesized in house by suspension precipitation method [26, 27]. In the present work, the precursor materials were calcium oxide (CaO) and phosphoric acid (H_3PO_4). Initially, CaO was dispersed in distilled water with a fixed volumetric ratio of CaO and water (18.6 g/l). The dispersed medium was kept on a hot plate and the suspension was stirred by magnetic stirrer. Following this, an appropriate concentration (0.15 M) of H_3PO_4 solution was added drop wise in the dispersed CaO medium. The temperature was kept at 80°C. The total solution was kept stirring for 3–4 h, to allow the completion of the reaction. After the reaction, the pH of the solution was adjusted to 10–12 by adding NH_4OH solution. Subsequently, the solution was kept for one day to precipitate the reaction product, which was collected by filtration using commercial filter paper. The precipitate was dried at 100°C for 24 h and subsequently, calcined at 800°C for 2 h. X-ray diffraction (XRD) of as- synthesized HAp, calcined at 800°C revealed the X-ray peaks corresponding to pure HAp phase. ICP-AES (Inductive coupled plasma-atomic emission spectroscopy: spectroflame modula FTM08, Germany) analysis using complexometry technique was performed to determine the Ca/P ratio of synthesized powder. A Ca/P atomic ratio of 1.64 was obtained from the HAp powder calcined at 800°C. It is important to note that pure stoichiometric HAp possesses a Ca/P atomic ratio of 1.67. Thus the HAp synthesized in the present study can be considered as phase pure and stoichiometric.

Mullite powder was procured commercially ($D_{30} \sim 0.67$ μm, $D_{50} \sim 1.04$ μm and $D_{99} \sim 2.39$ μm, KCM Corporation, Japan) and was used as second phase reinforcement. Different amount of mullite (10–30) wt% was mixed with HAp powder. The HAp-mullite composite powder mix was ball-milled for 16 h and then subsequently pressed in the form of pellets. In a similar way pellets of pure HAp and pure mullite were also made to compare the results. The sintering parameters were optimized based on the bulk density measurements and microstructure observations. The details of the densification, microstructure and process optimization could be found elsewhere [12]. Based on the sintering studies, all the three composite samples were sintered (pressureless) at 1,350°C for 2 h; where as pure HAp and pure mullite were sintered at 1,200°C for 2 h and 1,700°C for 4 h, respectively. The density values and sintered phases for the present set of samples are presented in Table 1. Subsequently, the sintered samples were smoothly polished using common ceramographic techniques and the polished samples were fretted in a ball-on-flat type fretting tribometer [make: DUCOM, Bangalore, India]. Here the samples acted as flat materials and sintered zirconia balls were used as counterbody materials. In the present instrumental set up, the ball was kept stationary and the flat samples had a reciprocatory motion. The frequency of this motion was kept constant for all the samples and in the present set of experiments the frequency was set as 5 Hz. The normal load applied on the ball was 10 N in all cases. All the experiments were performed for 100,000 cycles at a stretch. The schematic diagram of ball on flat configuration is shown in Fig. 1. Here the test samples were pure HAp, HAp-mullite composites and pure mullite. The frictional force was recorded using commercial software provided by the supplier. All the samples were fretted in dry ambient condition (27°C, 42% RH) as well as in SBF with added protein (albumin fraction 5; 5 g crystal powder/l). The SBF solution was prepared using the previously described method [28]. In actual body fluid the presences of various proteins (albumin, globulin etc.) can be found. Therefore, albumin has been being used for various in vitro mineralization and dissolution experiments [29]. In the present investigation 5 g/l albumin crystals of fraction 5 was dissolved in SBF.

Table 1 The densification, sintering conditions and phases present after sintering are mentioned against the sample designation

Samples	Maximum achievable densification (w.r.t. initial composition, %)	Sintering temperatures (°C)	Phases present
Pure HAp	99.17	1,200 for 2 h	HAp-ss
HAp-10 M	94	1,350 for 2 h	α-TCP-ss, HAp-ss, β-TCP-w, Mullite-ww, CaO-ww
HAp-20 M	98.1	1,350 for 2 h	α-TCP-s, β-TCP-ss, HAp-ww, Mullite-w, Gehlenite-ww, CaO-ww, Alumina-ww
HAp-30 M	95.6	1350 for 2 h	β-TCP-ss, HAp-ww, Mullite-s Gehlenite-ww, CaO-ww, Alumina-s
Pure mullite	98.7	1,700 for 4 h	Mullite-ss

The phases present in the sintered body are summarized based on the XRD peak intensities*ss* very strong, *s* strong, *ww* very weak, *w* weak

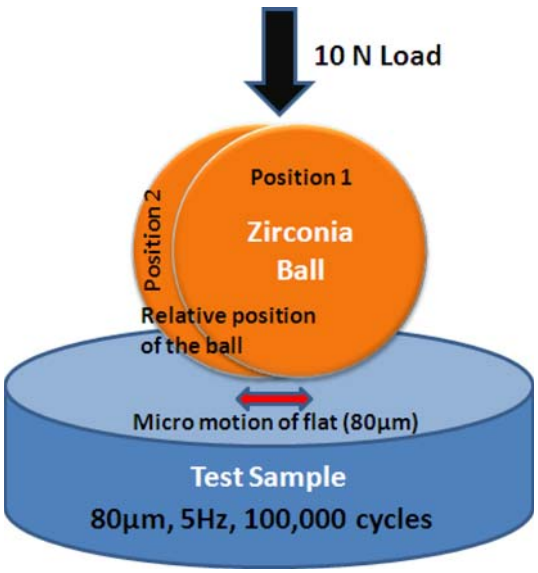

Fig. 1 Schematic representation of fretting mode I (ball-on-flat configuration) test, showing experimental fretting parameters for HAp-xMullite and Mullite samples (pressureless sintering at 1,350°C for 2 h) against ZrO_2 ball. The Half cycle travel length is 80 µm

After the fretting experiments, the worn samples were ultrasonically cleaned to remove the loosely attached wear debris and then scanned under laser surface profilometer (LSP). The fretted zone was scanned three dimensionally to obtain the wear volume of the samples. At the same time the maximum wear depths were also calculated from the 2-D profile taken at the middle of the wear scar. The area created due to the fretting action under each 2-D profile was calculated from LSP and then the areas were integrated throughout the wear scar zone. Thus the actual wear volume was calculated. After that the samples were coated with gold and subsequently the fretted zone was observed under scanning electron microscope (SEM-EDS: FEI, Philips). The topographical feature of the worn surface was recorded and critically analyzed. Hardness of the samples was measured by Vickers microhardness (instrumented). The details of the hardness measurements and other mechanical properties can be found elsewhere [12]. The contact pressure during fretting was calculated using various established models [30].

3 Results

3.1 COF data

The COF values are plotted against the number of cycles for various samples in Fig. 2. In the following, a comparison in steady state COF is being made. Figure 2a shows the variation in COF when fretted in air (dry), whereas Fig. 2b plots the variation of COF in SBF environment. In ambient condition, pure HAp showed minimum COF (0.35), whereas maximum COF (0.62) was recorded from pure mullite sample. All the HAp-mullite composite samples (i.e. 10, 20 and 30 wt%) showed similar values of COF (0.5) in steady state condition. During steady state period, noticeable fluctuations were observed. In dry condition, the COF values followed the following order:

$$PureMullite > HAp\text{-}10M, HAp\text{-}20M, HAp\text{-}30M > PureHAp$$

From Fig. 2b, the plotted COF values reveal that like in dry condition, pure HAp possessed lowest COF value ($\sim$0.3). However, HAp-10 M exhibited maximum COF of 0.55. A steady state COF of 0.45 and 0.4 was recorded for HAp-20 M and HAp-30 M composites, respectively. Pure mullite possessed COF of 0.5, which was lower than that in dry condition (0.6). Therefore, in SBF condition, COF followed the following order:

$$HAp\text{-}10M > PureMullite > HAp\text{-}20M > HAp\text{-}30M > PureHAp$$

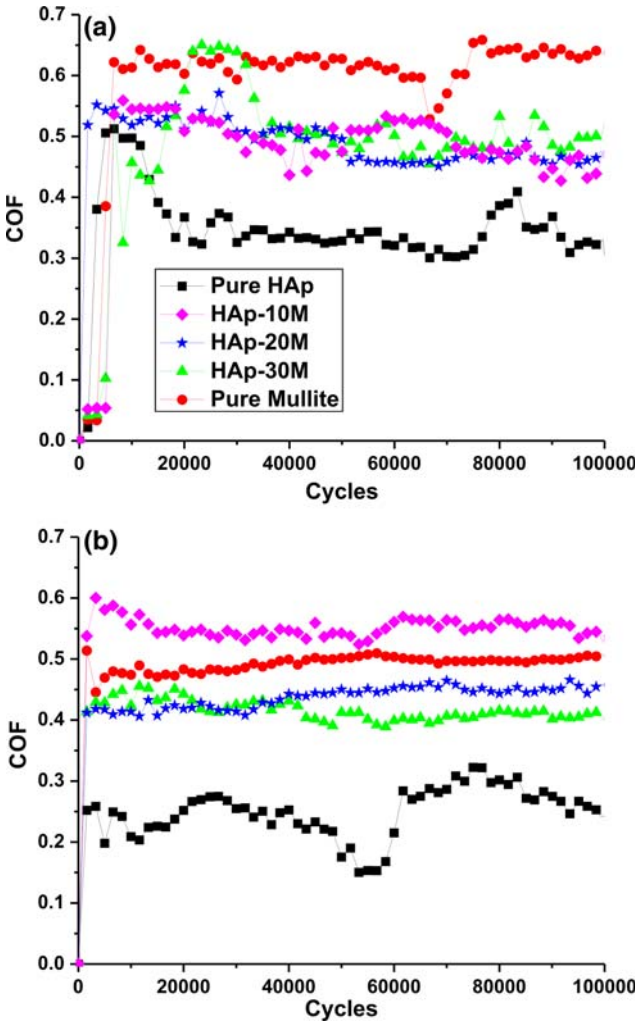

Fig. 2 Plots of coefficient of friction (COF) vs. number of fretting cycles for HAp-Mullite composites in **a** dry ambient condition **b** simulated body fluid with albumin protein environment

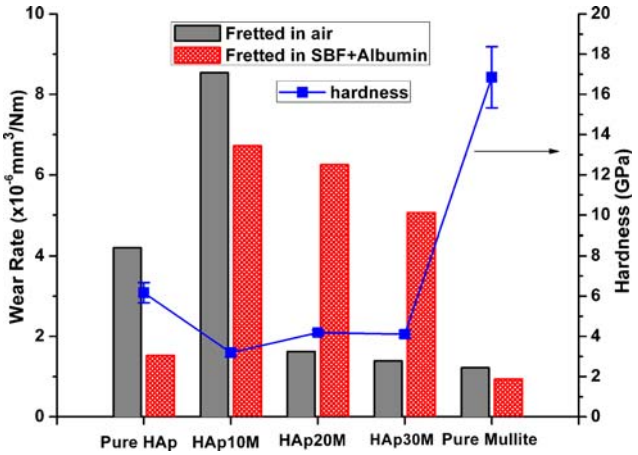

Fig. 3 Wear rate of different samples (pure HAp, HAp-mullite composites and pure mullite) are plotted when fretted in dry as well as in SBF + albumin medium. Around 10% deviation of the mean wear rate was measured in our experiments

3.2 Wear rate

The measured wear rate values are plotted in Fig. 3. Hardness values of the developed composite are also plotted in Fig. 3. In dry condition, the maximum wear rate (8.54×10^{-6} mm^3/Nm) was found for HAp-10 M sample. Pure mullite showed best wear resistance properties with the lowest wear rate of 1.22×10^{-6} mm^3/Nm. Pure HAp, HAp-20 M and HAp-30 M experienced wear rates of 4.2×10^{-6}, 1.62×10^{-6} and 1.39×10^{-6} mm^3/Nm respectively.

In SBF condition, the minimum wear rate (0.94×10^{-6} mm^3/Nm) was recorded for pure mullite. Pure HAp and HAp-10 M samples showed better wear resistance in SBF condition than dry contact with wear rate being measured as 1.53×10^{-6} mm^3/Nm and 6.72×10^{-6} mm^3/Nm, respectively. Interestingly, for HAp-20 M and HAp-30 M samples, the wear rates were higher in SBF medium than that of dry contact. The calculated wear rates were 6.25×10^{-6} mm^3/Nm and 5.06×10^{-6} mm^3/Nm for HAp-20 M and HAp-30 M samples, respectively. Fig. 4 shows the representative 2D depth profiles, recorded at the center of the wear scar on pure HAp, HAp-10 M–30 M and pure mullite after fretting tests in dry (Fig. 4a) as well as SBF condition (Fig. 4b). A closer look at Fig. 4a and b reveals the following information: (a) The worn surface of pure HAp was very rough (number of hills and valleys in 2D profile) independent of dry/SBF environment; (b) for HAp-10 M–30 M composites, the wear test in SBF environment produced very smooth surface compared to that in dry atmosphere; (c) Overall, 2D profiles corroborate well with the wear rate and wear depth data. Fig. 5 presents maximum fretting depth measured from the surface profile of 2-D scan. In dry condition, maximum wear depth of $\sim$20 μm was measured for pure HAp. For other samples the wear depth decreased gradually and for pure mullite, it showed least value ($\sim$2.5 μm). Similar trend was also observed in SBF condition except for HAp-10 M sample. In general, the wear depth values were consistently higher in dry conditions than in SBF medium.

3.3 Topographical observations of worn surface

As observed under SEM, the fretted areas are presented in Fig. 6 for a few selected samples in dry condition. Fig. 6 a, b; c, d and e, f present wear scar microstructure for pure HAp, HAp-20 M and HAp-30 M samples, respectively. The circles in Fig. 6a, c, and e indicate the fretting damage zone. Figure 6a shows delamination of the surface layer of HAp, whereas Fig. 6b shows the underlying fretted zone at higher magnification (×5000). Figure 6b clearly shows

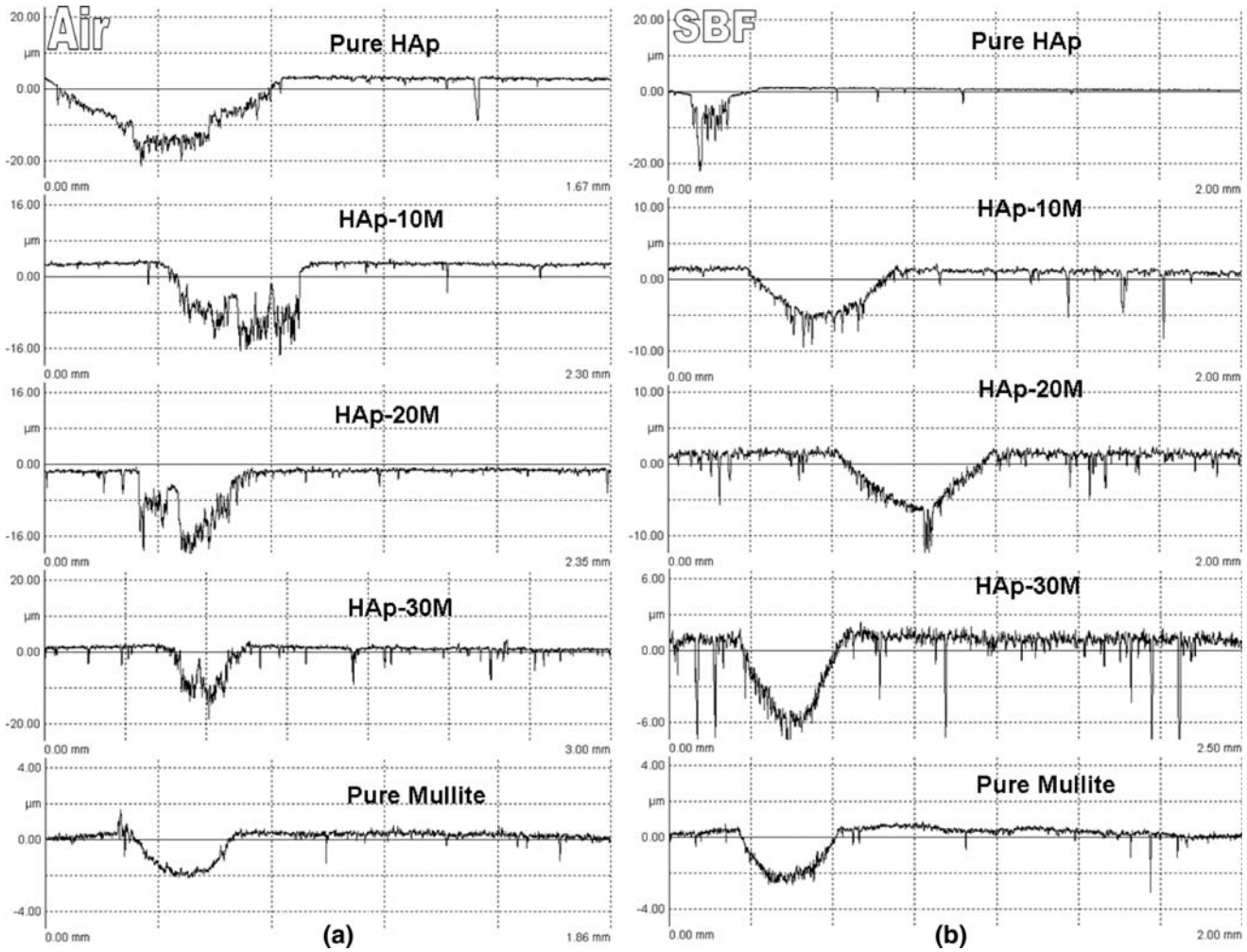

Fig. 4 2D wear depth profiles for pure HAp, HAp-30 M and pure mullite after fretting wear test in dry and SBF conditions

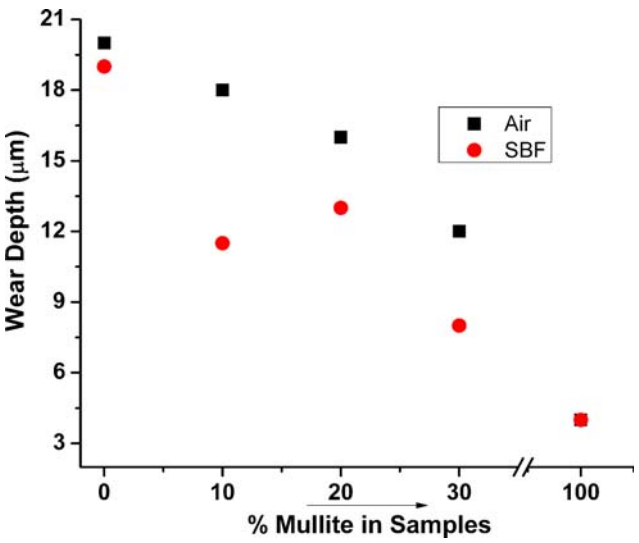

Fig. 5 Measured wear depth for various mullite-containing samples fretted in dry as well as in SBF conditions

that the wear was mainly dominated by ploughing action with microcracks formed perpendicular to the fretting direction. For HAp-20 M sample, fatigue cracks were also generated in addition to ploughing abrasion (Fig. 6c and d). However, the fatigue cracking was greatly reduced for HAp-30 M (Fig. 6f). EDS analysis of the worn surfaces is shown in the inset in Fig. 6b and d. The counterbody element, i.e. Zr could not be found in EDS analysis. For HAp-10 M sample, more severe wear and cracking was found and for pure mullite presence of only abrasive wear scratches were found.

However, for SBF condition, the wear mechanism was mainly dominated by abrasive scratches. Figure 7a, b, c and d show fretted microstructure for HAp-10 M, HAp-20 M, HAp-30 M and pure mullite samples. For HAp-10 M and 20 M samples, the wear damaged zones were characterized by abrasive scratches with mild fatigue cracking. This kind of cracking might occur on the deposited apatite layer due to post-experiment drying. However, for HAp-30 M

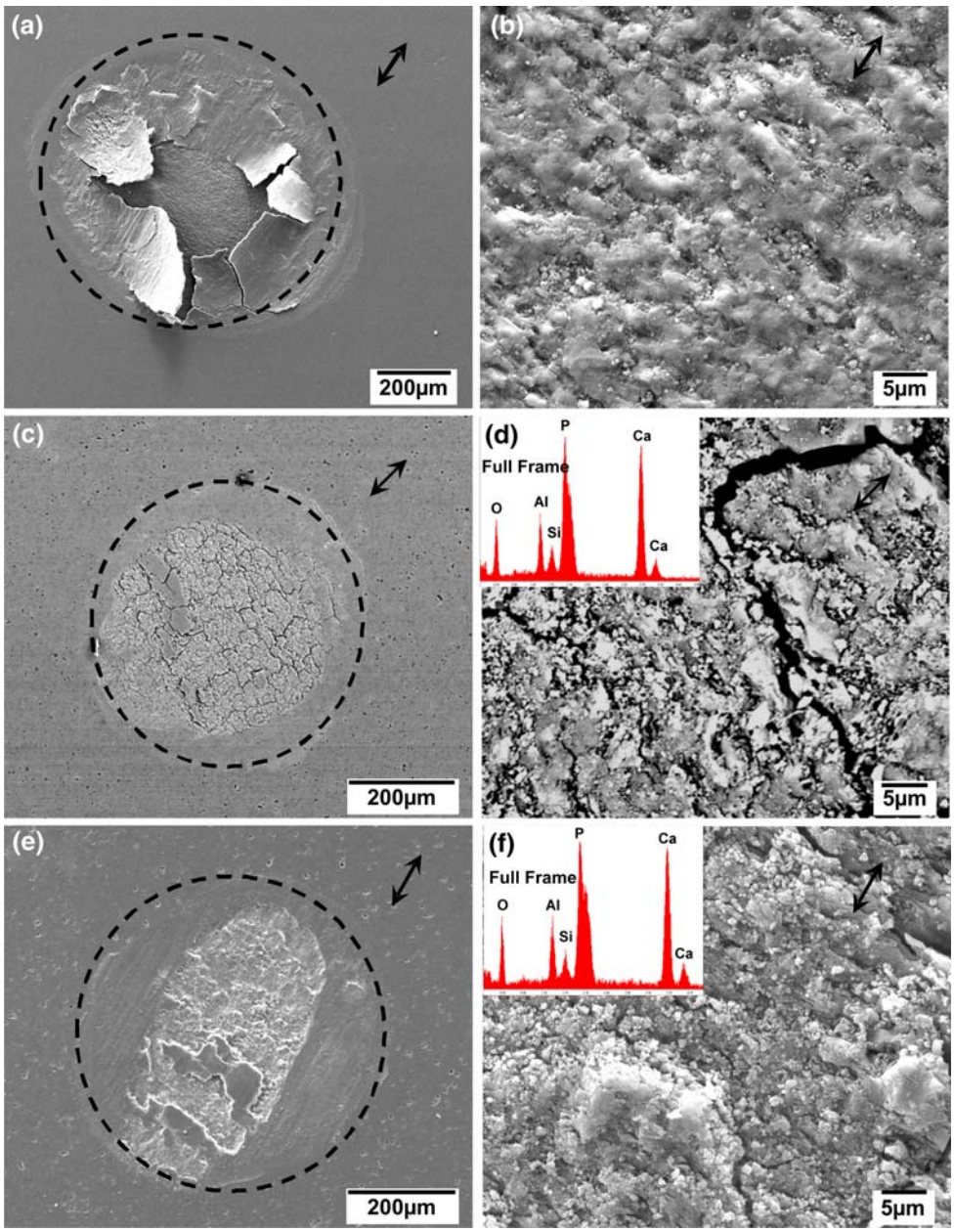

Fig. 6 SEM images of worn surfaces of **a**, **b** pure HAp sintered at 1,200°C, **c**, **d** HAp-20 M, and **e**, **f** HAp-30 M sintered at 1,350°C, after testing against zirconia in air. The double pointed arrow indicates fretting direction

samples the wear mechanism was mainly driven by ploughing and grain pullout. For pure mullite sample, the fretted surface showed only abrasive scratches. Similar to the previous case (dry contact), counterbody wear could not be observed in the fretted area. Also, the presence of various salts and proteins could not be found on the surface.

4 Discussion

4.1 Frictional behavior

In this subsection, an attempt has been made to explain the difference in friction and wear behavior. Pure HAp and pure mullite possess the lowest and highest COF values respectively and all the three composites show COF values intermediate to these. In dry condition, the formation of wear debris and their escape/displacement from the contact zone during fretting can cause fluctuations in COF which is evident in Fig. 2a. This process is quite smooth and steady in lubricated conditions thus leading to a COF curve with minimal fluctuations (except for pure HAp) as shown in Fig. 2b. It has to be mentioned here that fretting wear has characteristic potential of forming considerable amounts of very fine oxide debris and these wear debris particles often govern the wear of the materials [31, 32]. The Young's modulii of HAp-xM composites are inferior compared to that of pure HAp (~120 GPa) and pure mullite (240 GPa)

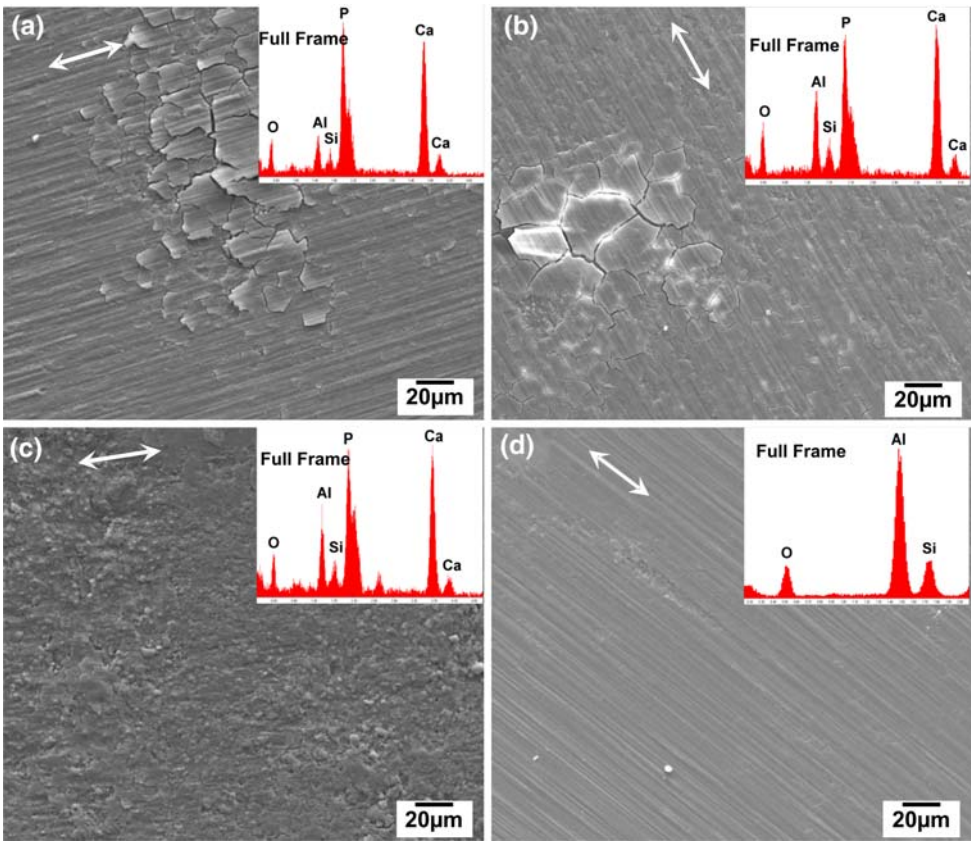

Fig. 7 SEM images of worn surfaces of **a** HAp-10 M sintered at 1,350°C, **b** HAp-20 M, sintered at 1,350°C, **c** HAp-30 M sintered at 1,350°C and **d** Pure Mullite sintered at 1,700°C, after testing against zirconia in SBF medium containing Albumin. The double pointed arrow indicates fretting direction

samples. Due to this lower elastic modulus values (~45–70 GPa), the initial contact diameter was higher (Table 2) than contact diameters of other materials. The strong asperity contact between mullite and zirconia counterbody was responsible for the highest COF for pure mullite samples. The data in Table 2 also indicate that the tests were conducted with variation in contact stress of ~809–1,038 MPa. This kind of contact pressure is much higher than the upper end of the commonly experienced contact pressure at various orthopedic joints (Hip joint, maximum contact pressure ~25 MPa) [33].

The COF values seem to be quite strange in SBF environment! The highest COF values recorded for HAp-10 M sample can be attributed to the dominant presence of α-TCP phase (Table 1). In the presence of SBF medium and constant fretting action, α-TCP can be dissolved locally at the contact and therefore, causes localized spalling, leading to an increase in COF. This type of phenomenon was not observed in case of HAp-20 M and HAp-30 M samples as the major phase is β-TCP. It is already well-known that β-TCP is more stable than α-TCP in body fluid. Except for HAp-10 M samples, the lowering of COF in SBF condition compared to dry contact can be attributed to the lubricating action of SBF solution. Considering various parameters, the liquid film at the contact would be in the boundary regime and hence the lubrication effect wound not be much. The real asperity contact can not be avoided in spite of the presence of liquid film.

4.2 Wear mechanism

In this section, the wear mechanisms are analyzed on the basis of wear scar microstructure and Hertzian contact stress conditions. An effort will be made to discuss the effect of fretting environment (ambient and SBF lubrication) on the wear mechanisms.

Following the Hertzian contact mechanics theory [34], the initial contact pressure (maximum and mean) are calculated. The maximum and mean contact pressures along with initial Hertzian contact diameter are tabulated in Table 2. Hertzian contact pressure and contact diameter are mainly functions of elastic modulus of the mating materials. Having highest E-modulus value, mullite possesses very high contact pressure (1,038 MPa) and lowest contact diameter (136 μm). The contact pressure is lowest (521 MPa) and the diameter is highest (192 μm) for HAp-10 M composite, as it possesses lowest Young's modulus values (45 GPa). The low modulus materials tend to reduce contact pressure by increasing the contact diameter. After the fretting experiments, the wear scar diameters were increased due to the oscillatory motion and consequently the contact pressures were getting reduced. In dry contact,

Table 2 Maximum and mean Hertzian contact pressures as well as the initial Hertzian contact diameter for the investigated fretting couple (containing pure HAp, pure Mullite, and HAp-mullite composites) are presented along with measured wear scar diameter

Material	Medium	Maximum Hertzian contact pressure (initial) (MPa)	Mean Hertzian contact pressure (initial) (MPa)	Initial Hertzian contact diameter (μm)	Measured wear scar diameter (μm)	E-modulus (GPa)
Pure HAp	Dry	809	540	153.7	767	120
	SBF	809	540	153.7	377	
HAp-10 M	Dry	521	347	191.6	801	45
	SBF	521	347	191.6	671	
HAp-20 M	Dry	621	414	175.4	564	72
	SBF	621	414	175.4	636	
HAp-30 M	Dry	597	398	178.9	563	68
	SBF	597	398	178.9	614	
Pure mullite	Dry	1038	692	135.7	530	240
	SBF	1038	692	135.7	344	

the fretted contact diameters (Table 2) are proportional to the initial contact diameter. However, in SBF medium discrepancy was found for HAp-20 M and HAp-30 M samples. In these two cases, the fretted wear scar diameters were higher than that of dry contact. Therefore, the higher wear rate for these two composites in SBF medium than that of dry condition can be understood. These two composites mainly contained β-TCP and the wear resistance of β-TCP is inferior in SBF medium.

In dry contact, the wear of pure HAp mainly occurred by delamination and microcrack formation. The high contact pressure (809 MPa) was sufficient to initiate the microcracks at the contact region. Also, being very brittle material (toughness: $\sim$0.6 MPam$^{0.5}$), HAp could easily form microcracks at the fretting contact. The microcracks were also generated at the subsurface region. Due to prolonged cyclic loading action, the microcracks grew and combined to each other culminating delamination of the surface layer. For HAp-10 M and HAp-20 M composites, the fatigue cracks were formed due to the cyclic loading over prolonged time (Fig. 6). For HAp-30 M composites, the extent of fatigue cracks was very less. Here, the grains were pulled out mainly due to the ploughing action of the counterbody asperities. For pure mullite, the counterbody asperities plastically deformed the surface, resulting in abrasive scratches due to very high contact pressure.

In SBF condition, (Fig. 7) the contact damage was considerably less than that of dry contact. Due to the presence of liquid film, only abrasion (except for HAp-30 M), and mild ploughing occurred. However, the wear debris formed in SBF condition was constantly flushed off due to the rapid vibrating motion at contacts. For the samples containing TCP phase, such effect was more prominent as the TCP phase has higher solubility than pure HAp or mullite. Therefore, the wear rate was increased to some extent. Even for HAp-20 M and HAp-30 M samples, the wear rates exceeded the value obtained in dry contact.

The wear depth values presented in Fig. 5 do not exactly follow the wear rate trends. The reason is that wear rate depends on both wear depth as well as wear scar diameter. Lower depth but larger wear scar may produce higher wear rate. For HAp-20 M and HAp-30 M samples though the wear depth values were lower in case of SBF condition than in dry condition, the wear rate values were higher due to larger wear scar diameter (Table 2). In these two composites, the amount of reaction product was higher than that of other samples. The sintered reaction product, Gehlenite, present in the grain boundary region became plastic mass when hydrated in SBF condition. Therefore, the fretted zone could be plastically deformed and hence the wear scar diameter was increased.

The effect of albumin present in SBF needs to be analyzed. As a direct observation from SEM, it is revealed that albumin did not adhere or got absorbed on the fretted zone. It is possible that due to continuous reciprocatory motion at the fretting contact, it was difficult for protein molecules to be adhered on the surface. Also, if there was some adherence that might be very loosely bonded which was washed away during cleaning of samples after the experiments. However, albumin might play an important role in controlling the wear rate and COF during fretting experiments. Marques et al. [29] studied the effect of albumin on mineralization process in Hank's balanced salt solution (HBSS). From their results, it was revealed that albumin helps in TCP dissolution due to its Ca affinity in aqueous HBSS solution. On account of similar reason, serum albumin inhibited apatite crystal growth on the sample surface in SBF solution [35–37]. Similar results were also obtained from the work of Wang et al. [38]. Their results showed that at concentration of 40 g/L, bovine serum albumin has significant retardation effect on apatite precipitation from SBF onto pure or fluoridated HA coatings. However, Marques et al. [29] concluded that depending on the sample composition and followed by pre-adsorbed

Table 3 Summary of literature results on various HAp based materials undergone fretting wear damage in different medium. For comparison, the present research results are also mentioned. The testing conditions are also indicated

Materials	Counter body	Medium of testing	Experimental conditions	COF	Wear rate	Mechanism of wear	References
HAp-PSZ	UHMWPE	Human plasma	Pin-on-disc Load 4.3 N	0.04–0.06	$5.9 \pm 0.7 \times 10^{-9}$ mm^3/Nm	Fatigue wear	[38]
HAp-Collagen with 10% Hyaluronic acid	Stainless steel	Carboxymethyle Cellulose solution	Pin-on-disc Load 10-70 N	0.01–0.04	4.1×10^{-5} mm^3/Nm	Deformation and fracture of HA layer, Transfer layer build up	[39]
		Bovine serum		0.01–0.03	–		
HAp-CNT	ZrO_2	*c*-SBF	Pin-on-disc Load 8.8 N	–	38.9 g $m^{-2}/10^4$ revolutions	Abrasion, fracture, plastic deformation fragmentation, chipping and ploughing	[40]
HAp-NFSS	Unknown	Air	Pin-on-disc Load 15, 45 N	0.5–0.85 (15 N) 0.35–0.75 (45 N)	–	Abrasive wear at low load; Abrasive, Adhesive and third body mechanism at higher load	[41]
HDPE-HAp-Al_2O_3	Stainless steel	Hanks balanced salt solution (HBSS)	Ball-on-flat (Fretting) Load 10 N	0.07–0.11	$2.3 \pm 0.7 \times 10^{-6}$ mm^3/Nm	Mild abrasive wear and limited plastic deformation	[42]
HDPE-HAp-Al_2O_3	Al_2O_3	SBF	Ball-on-flat (fretting) Load 10 N	0.11	$5.9 \pm 0.9 \times 10^{-7}$ mm^3/Nm	Mild abrasive wear and limited plastic deformation	[43]
HDPE-HAp-Al_2O_3	ZrO_2	SBF	Ball-on-flat (fretting) Load 10 N	0.05	$1.1 \pm 0.7 \times 10^{-6}$ mm^3/Nm	Mild Abrasive wear and limited plastic deformation	[44]
HAp-30 wt% Mullite	ZrO_2	SBF	Ball-on-flat (fretting) Load 10 N	0.4	5×10^{-6} mm^3/Nm	Mild ploughing	Current study
HAp	Hardened SS	Dry	Ball-on-flat Load 10 N	0.7–0.8	$1.36–11.5 \times 10^{-6}$ mm^3/Nm	Delamination and abrasive wear	[15]

albumin on the surface, the apatite formation kinetics even became faster. From the above discussion, it is clear that albumin in general retards apatite formation on the sample surface in SBF. Apatite layer could also act as protective layer against further materials removal. Therefore, the wear rate of CaP-containing materials in SBF was found to be higher than expected, due to such inhibitory effect. However, in some places on the fretted microstructure, the apatite layer was found to be adhered discretely and later upon drying, the layer was cracked. SEM images probably show the presence of apatite with signature of cracking due to drying. For pure mullite, this kind of effect was not observed as pure mullite did not induce any apatite layer formation, when immersed in SBF solution.

A comparison of the tribological results obtained with pure HAp and HAp based composites, as reported in literature is presented in Table 3. Broadly, the wear rate varies between 10^{-5} and 10^{-9} mm^3/Nm depending on operating parameters. Difference between COF and wear rate, as observed from Table 3, can be explained on the basis of difference in tribological environment as well as counterbody. Although coefficient of friction as recorded with HAp-mullite composites was on the higher side compared to other competing materials; the wear rate, varying in the order of 10^{-6} mm^3/Nm showed good wear resistant properties. Summarily, mild abrasion, fracture and fatigue wear were reported as dominant wear mechanisms for different HAp based composites.

A rise in contact temperature plays an important role in determining tribological behavior of the materials. However, in the present case the contact temperature rise could not be calculated due to the unavailability of the thermal conductivity data of the composite materials. In some earlier experiments [23, 25] on various set of materials it was already shown that the contact temperature rise was very less in fretting contact due to its lower sliding velocity. Hence, the temperature would not be a major factor in case of fretting contacts.

5 Conclusions

Based on the experimental results and their discussion, the following conclusions can be drawn:

(a) The steady state COF values for pure HAp were always lower (0.30–0.35), irrespective of the fretting environment. In dry contact, the maximum COF value (0.6) was obtained for pure mullite ceramic and in SBF environment, HAp-10 wt% mullite composite shows highest COF value (0.55).

(b) In both dry and SBF environment, the wear rate varied within the same order of magnitude (10^{-6} mm^3/Nm). In case of dry contact, HAp-20% Mullite (1.6×10^{-6} mm^3/Nm) and HAp-30% Mullite composite (1.4×10^{-6} mm^3/Nm) exhibited better wear resistance than pure HAp (4.2×10^{-6} mm^3/Nm). No systematic trend between wear rate (dry contact) and hardness was observed. In SBF environment, the wear rate was noticeably reduced in case of pure HAp, mullite and HAp-10 M composite. The wear depth varied between 2 and 20 μm with higher depth being consistently measured in case of dry contact.

(c) In dry contact, the wear mechanism was mainly guided by microcracking, delamination, ploughing and fatigue cracking. However, in SBF medium, the major wear mechanism for the mullite-containing HAp composites was found to be mild abrasion and/or ploughing.

(d) Based on comparison among investigated composite materials, HAp—30 wt% mullite sample appears to have the best combination of COF and wear resistance in dry and SBF conditions.

Acknowledgements The authors would like to thank Department of Biotechnology, Govt. of India for the financial support.

References

1. Betts F, Blumenthal NC, Posner AS. Bone mineralization. J Cryst Growth. 1981;53:63–73.
2. Suzuki T, Ohashi R, Yokogawa Y, Nishizawa K, Nagata F, Kawamoto Y, et al. Initial anchoring and proliferation of fibroblast L-929 cells on unstable surface of calcium phosphate ceramics. J Biosci Bioeng. 1999;87:320–7.
3. Chen QZ, Wong CT, Lu WW, Cheung KMC, Leong JCY, Luk KDK. Strengthening mechanisms of bone bonding to crystalline hydroxyapatite in vivo. Biomaterials. 2004;25:4243–54.
4. Balcik C, Tokdemir T, Senkoylu A, Koc N, Timucin M, Akin S, et al. Early weight bearing of porous HA/TCP (60/40) ceramics in vivo: a longitudinal study in a segmental bone defect model of rabbit. Acta Biomater. 2007;3:985–96.
5. Gautier S, Champion E, Assollant DB. Processing, microstructure and toughness of Al_2O_3 platelet-reinforced hydroxyapatite. J Eur Ceram Soc. 1997;17:1361–9.
6. Li J, Fartash B, Hermansson L. Hydroxyapatite—alumina composites and bone-bonding. Biomaterials. 1995;16:417–22.
7. Rao RR, Kannan TS. Synthesis and sintering of hydroxyapatite–zirconia composites. Mater Sci Eng. 2002;20:187–93.
8. Silva VV, Lameiras FS, Domínguez RZ. Microstructural and mechanical study of zirconia-hydroxyapatite (ZH) composite ceramics for biomedical applications. Compos Sci Technol. 2001;61:301–10.
9. Gollera G, Demirkıran H, Oktar FN, Demirkesen E. Processing and characterization of bioglass reinforced hydroxyapatite composites. Ceram Int. 2003;29:721–4.
10. Suchanek W, Yashima M, Kakihana M, Yoshimura M. Hydroxyapatite/hydroxyapatite-whisker composites without sintering additives: mechanical properties and microstructural evolution. J Am Ceram Soc. 1997;80:2805–13.

11. Nath S, Biswas K, Basu B. Phase stability and microstructure development in hydroxyapatite-mullite system. Scr Mater. 2008;58:1054–7.
12. Nath S. Development of novel calcium phosphate-mullite composites for orthopedic applications, PhD thesis, IIT Kanpur, India, 2008.
13. Nath S, Basu B, Mohanty M, Mohanan PV. In vivo response of novel Hydroxyapatite-mullite composites: results up to 12 weeks of implantation. J Biomed Mater Res B. 2009;90B:547–57.
14. Schaaff P. The role of fretting damage in total hip arthroplasty with modular design hip joints-evaluation of retrieval studies and experimental simulation methods. J Appl Biomater Biomech. 2004;2:121–35.
15. Fu Y, Batchelor AW, Khor KA. Fretting wear behavior of thermal sprayed hydroxyapatite coating lubricated with bovine albumin. Wear. 1999;230:98–102.
16. Choubey A, Basu B, Balasubramaniam R. Tribological behavior of Ti-based alloys in simulated body fluid solution at fretting contacts. Mater Sci Eng A. 2004;379:234–9.
17. Sheeja D, Tay BK, Lau SP, Nung LN. Tribological characterization of diamond-like carbon coatings on Co–Cr–Mo alloy for orthopedic applications. Surf Coat Technol. 2001;146–147: 410–6.
18. Sheeja D, Tay BK, Nung LN. Tribological characterization of surface modified UHMWPE against DLC-coated Co–Cr–Mo. Surf Coat Technol. 2005;190:231–7.
19. Hauert R, Müller U. An overview on tailored tribological and biological behavior of diamond-like carbon. Diam Relat Mater. 2003;12:171–7.
20. Nath S, Bodhak S, Basu B. Tribological investigation of Novel HDPE-HAp-Al_2O_3 hybrid biocomposites against Steel under Dry and Simulated Body Fluid Condition. J Biomed Mater Res A. 2007;83A:191–208.
21. Nath S, Sinha N, Basu B. Microstructure, mechanical and tribological properties of microwave sintered Ca-stabilized zirconia for biomedical applications. Ceram Int. 2008;34:1509–20.
22. Bodhak S, Nath S, Basu B. Understanding the fretting wear properties of HAp, Al_2O_3-containing HDPE biocomposites against ZrO_2. J Biomed Mater Res A. 2008;85A:83–98.
23. Nath S, Bajaj S, Basu B. Microstructure, mechanical and tribological properties of microwave sintered Mg-doped zirconia. Int J Appl Ceram Technol. 2008;5:49–62.
24. Nath S, Bodhak S, Basu B. HDPE-Al_2O_3-HAp composites for biomedical applications: processing and characterization. J Biomed Mater Res B Appl Biomater. 2009;88B:1–11.
25. Bodhak S, Nath S, Basu B. Friction and wear properties of novel HDPE -HAp-Al_2O_3 composites against alumina counterface. J Biomater Appl. 2009;23:407–33.
26. Rathje W. Zurkentnis de phosphate I. flubber hydroxyapatite. Bodenk Pflernah. 1939;12:121–8.
27. Santos MH, Oliveira M, Souza LPF, Mansur HS, Vasconcelos WL. Mater Res. 2004;7:625–30.
28. Oyane A, Kim HM, Furuya T, Kokubo T, Miyazaki T, Nakamura T. Preparation and assessment of revised simulated body fluids. J Biomed Mater Res A. 2003;65A:188–95.
29. Marques PAAP, Serro AP, Saramago BJ, Fernandes AC, Magalh MCF, Correia RN. Mineralisation of two phosphate ceramics in HBSS: role of albumin. Biomaterials. 2003;24:451–60.
30. Archard JF. The temperature of rubbing surfaces. Wear. 1959;2: 438–55.
31. Varenberg M, Halperin G, Etsion I. Different aspects of the role of wear debris in fretting wear. Wear. 2002;252:902–10.
32. Singer IL. How third-body processes affect friction and wear. MRS Bull. 1998;23:37–40.
33. Kumagai M, Kim YH, Inoue N, Genda E, Hua K, Liong BTL, Koo T, Chao Y. 3-D Dynamic Hip Contact Pressure Distribution in Daily Activities. Summer Bioengineering Conference, June 25–29, Sonesta Beach Resort in Key Biscayne, Florida 2003; 53–54.
34. Bhushan B. Principles and applications of tribology. A Wiley-Interscience Publication, John Wiley & Sons, INC. 605 Third Avenue, New York, NY 10158-0012, pp 201–202.
35. Gilman H, Hukins DWL. Seeded growth of hydroxyapatite in the presence of dissolved albumin at constant composition. J Inorg Biochem. 1994;55:31–9.
36. Garnett J, Dieppe P. The effects of serum and human albumin on calcium hydroxyapatite crystal growth. Biochem J. 1990;266: 863–8.
37. Serro AP, Fernandes AC, Saramago B, Lima J, Barbosa MA. Apatite deposition on titanium surfaces—the role of albumin adsorption. Biomaterials. 1997;16:963–6.
38. Wang Q, Ge S, Zhang D. Nano-mechanical properties and biotribological behaviors of nanosized HA/partially-stabilized Zirconia composites. Wear. 2005;259:952–7.
39. Chowdhury SKR, Kulkarni AC, Basak A, Roy SK. Wear characteristic and biocompatibility of some hydroxyapatite-collagen composite acetabular cups. Wear. 2007;262:1387–98.
40. Balani K, Chen Y, Harimkar SP, Dahotre NB, Agarwal A. Tribological behaviour of plasma-sprayed carbon nanotube-reinforced hydroxyapatite coating in physiological solution. Acta Biomater. 2007;3:944–51.
41. Younesi M, Bahrololoom ME. Optimizations of wear resistance and toughness of HA/NFSS new bio-composites for using in total joint replacement. Mater Des. 2009;31:234–43.
42. Nath S, Bodhak S, Basu B. Tribological investigation of novel HDPE-HAp-Al2O3 hybrid biocomposites against steel under dry and simulated body fluid condition. J Biomed Mater Res Part A. 2007;83A:191–208.
43. Bodhak S, Nath S, Basu B. Friction and wear properties of novel HDPE-HAp-Al_2O_3 biocomposites against Alumina counterface. J Biomater Appa. 2009;23:407–23.
44. Bodhak S, Nath S, Basu B. Fretting wear properties of hydroxyapatite, alumina-containing high density polyethylene biocomposites against zirconia. J Biomed Mater Res Part A. 2008;85A:83–98.